iScience

CellPress

Article

ARAP1 Bridges Actin Dynamics and AP-3-Dependent Membrane Traffic in Bone-Digesting Osteoclasts

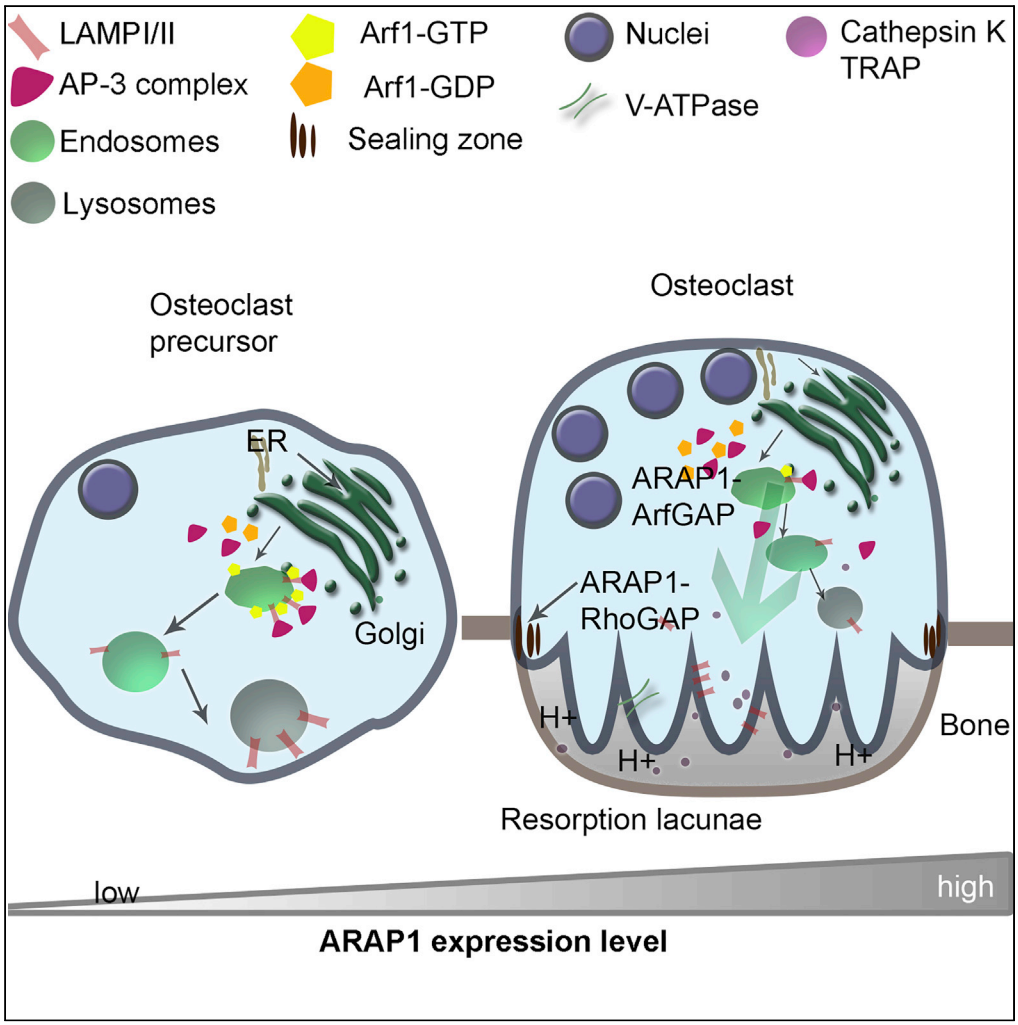

Sandra Segeletz, Lydia Danglot, Thierry Galli, Bernard Hoflack

bernard.hoflack@tu-dresden.de

HIGHLIGHTS

ARAP1 is a bridging factor controlling actin and membrane dynamics in osteoclasts

ARAP1 controls podosome dynamics and AP-3 coat recruitment to membranes

AP-3 controls targeting of lysosomal membrane proteins to the ruffled border

AP-3-deficient mocha mice develop osteoporosis

Segeletz et al., iScience 6, 199–211
August 31, 2018
https://doi.org/10.1016/j.isci.2018.07.019

iScience

CellPress

Article

ARAP1 Bridges Actin Dynamics and AP-3-Dependent Membrane Traffic in Bone-Digesting Osteoclasts

Sandra Segeletz,[1,3] Lydia Danglot,[2] Thierry Galli,[2] and Bernard Hoflack[1,4,*]

SUMMARY

Bone-resorbing osteoclasts play a central role in bone remodeling and its pathology. To digest bone, osteoclasts re-organize both F-actin, to assemble podosomes/sealing zones, and membrane traffic, to form bone-facing ruffled borders enriched in lysosomal membrane proteins. It remains elusive how these processes are coordinated. Here, we show that ARAP1 (ArfGAP with RhoGAP domain, ankyrin repeat and PH domain-containing protein 1) fulfills this function. At podosomes/sealing zones, ARAP1 is part of a protein complex where its RhoGAP domain regulates actin dynamics. At endosomes, ARAP1 interacts with AP-3 adaptor complexes where its Arf-GAP domain regulates the Arf1-dependent AP-3 binding to membranes and, consequently lysosomal membrane protein transport to ruffled borders. Accordingly, ARAP1 or AP-3 depletion in osteoclasts alters their capacity to digest bone *in vitro*. and AP-3δ-deficient *mocha* mice, a model of the Hermansky-Pudlak storage pool syndrome, develop osteoporosis. Thus, ARAP1 bridges F-actin and membrane dynamics in osteoclasts for proper bone homeostasis.

INTRODUCTION

Bone remodeling is the continuous process of bone digestion and rebuilding occurring throughout life. It is essential for the proper development, maintenance, and repair of the skeleton of vertebrates and is also central in bone pathology. It involves the coordinated activity of bone-building osteoblasts and bone-digesting osteoclasts to maintain bone mass. Osteoclasts originate from hematopoietic, mononucleated precursors, which upon their activation by the cytokines, macrophage-stimulating factor, and receptor activator of nuclear factor-κB ligand (RANKL), differentiate and fuse with each other to generate multinucleated osteoclasts (Teitelbaum, 2000). To digest the bone matrix, osteoclasts attach onto the bone surface and condense their podosomes, structural units linking cell adhesion molecules and actin meshworks, into podosomal belts to form a sealing zone. This sealing zone segregates the highly convoluted, bone-facing membrane, also known as ruffled border, from other membrane domains. This ruffled border and the bone surface limit the extracellular resorption lacunae, which are acidified to dissolve the inorganic bone matrix and are rich in secreted hydrolytic, lysosomal enzymes to digest the organic bone matrix.

Sealing zones and ruffled borders are highly dynamic structures. They are formed when osteoclasts attach onto bone surfaces and are then disassembled when osteoclasts move to other bone areas to digest. The ruffled border is highly enriched in lysosomal membrane proteins such as LAMPI, LAMPII, V-ATPase, and chloride channels, which are found normally in late endocytic compartments of other cell types (Palokangas et al., 1997; Akamine et al., 1993; Vaananen et al., 1990), and Rab7, a small GTPase, which normally regulates membrane traffic from early to late endocytic compartments (Palokangas et al., 1997; Zhao et al., 2002). The intracellular transport of newly synthesized membrane proteins from the biosynthetic pathway to the endosomal system relies on the hetero-tetrameric, AP-3 adaptor complex, one of the coat components regulating protein sorting in eukaryotes (Dell'Angelica et al., 1997). AP-3 interaction with its target membranes is tightly regulated by the Arf-1 GTPase (Ooi et al., 1998) and its corresponding guanine nucleotide exchange factors (GEFs) or GTPase-activating proteins (GAPs). How lysosomal membrane proteins are targeted to the ruffled border of osteoclasts is unknown, although a current view is that in osteoclasts secretory lysosomes can fuse with the plasma membrane to deliver their membrane components and discharge their hydrolytic, lysosomal enzymes into the resorption lacunae (Mulari et al., 2003; van Meel et al., 2011). However, other mechanisms may exist, for example, the endosomal recycling pathway that contributes to the efficient delivery to the ruffled border (Palokangas et al., 1997; Steenblock et al., 2014).

[1]Biotechnology Center, Technische Universität Dresden, Tatzberg 47-51, Dresden 01307, Germany

[2]Centre de Psychiatrie et Neurosciences, UMR-S894 INSERM, Université Paris Descartes, 102-108 rue de la Santé, Paris 75014, France

[3]Present address: Max Planck Institute of Molecular Cell Biology and Genetics, MPI-CBG, Pfotenhauerstrasse 108, Dresden 01307, Germany

[4]Lead Contact

*Correspondence: bernard.hoflack@tu-dresden.de

https://doi.org/10.1016/j.isci.2018.07.019

The formation of sealing zones is instrumental in ruffled border biogenesis. They result from the condensation of individual podosomal units consisting of F-actin cores linked to cell adhesion molecules, thereby forming large protein complexes containing paxillin, gelsolin, talin, filamin A, integrins, and many other proteins (Linder and Aepfelbacher, 2003). Podosome/sealing zone assembly and disassembly is regulated by GTPases of the Rho family (Buccione et al., 2004), in particular Cdc42, RhoA, and Rac (Heckel et al., 2009; Saltel et al., 2004; Chellaiah et al., 2000; Chellaiah, 2005). Their dynamics is also regulated by the Src kinase-dependent phosphorylation and activation of several podosomal components (Soriano et al., 1991), such as the Arf-6 GAP GIT2 (Heckel et al., 2009), the Cdc42 guanine exchange factor FGD6 (Steenblock et al., 2014), or the BAR-domain scaffolding protein proline-serine-threonine phosphatase-interacting protein (PSTPIP) 1 (Sztacho et al., 2016), which, as part of a protein complex with the tyrosine-protein phosphatase non-receptor type 6 and the phosphatidylinositol-3,4,5-trisphosphate 5-phosphatase 1/2, controls the local dephosphorylation of membrane phospholipids and Src-phosphorylated substrates at podosomes, thereby triggering their disassembly (Sztacho et al., 2016; Heckel et al., 2009).

How sealing zone and ruffled border assemblies are coordinated is largely unknown. Here, we illustrate the functional importance of the PSTPIP1/2 interactor ARAP1, an ArfGAP with RhoGAP domain, ankyrin repeat, and PH domain protein 1, in these processes. In different cell types, ARAP1 associates with various intracellular compartments and actin-related structures such as filopodia (Miura et al., 2002). In NIH 3T3 cells, ARAP1 regulates through Arf1/5 circular dorsal ruffles, which share many characteristics with podosomes (Hasegawa et al., 2012; Buccione et al., 2004). We now show that in osteoclasts ARAP1 regulates sealing zone assembly, most likely through its Rho GAP domain, and Arf1-dependent AP-3 binding to endosomal membranes, most likely through its ArfGAP domain, for delivery of lysosomal membrane proteins to the ruffled border. Thus, our study shows that ARAP1 coordinates sealing zone dynamics and ruffled border biogenesis to modulate bone resorption.

RESULTS

ARAP1 Expression during Osteoclastogenesis

We first assessed by western blotting the expression level of ARAP1 during the RANKL-induced differentiation of RAW264.7 macrophage-like cells into mature osteoclasts. We used an antibody recognizing the C-terminal part of murine ARAP1 conserved in all ARAP1 isoforms (Figure 1A). In RAW264.7 cells, this antibody recognized one major band corresponding to the size of isoform 3 (Figure 1B). Two smaller bands were detectable but only after long exposure times. They could be assigned to ARAP1 isoforms 1 or 4 as they disappeared upon ARAP1 knockdown (Figure S1A). ARAP1 isoform 2 was not detected by western blotting or qPCR using different primers designed for the specific 5′ UTR (data not shown). ARAP1 expression increased during the differentiation of mononucleated RAW264.7 cells with RANKL, reaching an ~10 fold increase at day 4 after RANKL treatment, when mature, multinucleated osteoclasts were observed (Figure 1C). This suggested that ARAP1 could play an important role in osteoclasts as seen for several other proteins strongly up-regulated during osteoclastogenesis such as the Src tyrosine kinase, the tartrate-resistant acid phosphatase TRAP, or the protease cathepsin K (Czupalla et al., 2005).

ARAP1 Interactome

To understand ARAP1 function in osteoclasts, we first identified ARAP1 binding partners. We immunoprecipitated with an anti-ARAP1 antibody the endogenous ARAP1 from an osteoclast lysate and identified its binding partners by semi-quantitative mass spectrometry. We identified 1,434 proteins with a threshold of 95%, of which ~150 were at least 2-fold enriched after immunoprecipitation (Table 1). These putative ARAP1 interactors first included the CIN85 (Cbl-interacting protein of 85 kDa) protein (also known as SH3 domain-containing kinase-binding protein 1 isoform 1), previously identified as an ARAP1 interactor by the yeast two-hybrid system and liquid chromatography-tandem mass spectrometry (LC-MS/MS) (Havrylov et al., 2009; Yoon et al., 2011). Second, several components of actin-rich podosomes were identified, e.g., subunits of the actin-related protein 2/3 complex, gelsolin, filamin-A, the F-actin capping protein complex, and the BAR-domain containing PSTPIP1/2, two key regulators of podosomes/sealing zones dynamics in osteoclasts (Sztacho et al., 2016). Thus, this analysis confirmed our previous studies showing that PSTPIP1 binds ARAP1 (Sztacho et al., 2016). Finally, the MS analysis of ARAP1 interactors identified several components involved in membrane traffic. This included the vacuolar protein sorting-associated protein 13 (VPS13), whose function is still poorly understood, and the four subunits of the adaptor complex 3, a coat component involved in lysosomal targeting of membrane proteins such as LAMP1 or LAMP2 (Peden et al., 2004). These findings also confirmed our previous studies showing that ARAP1 is part of a protein network

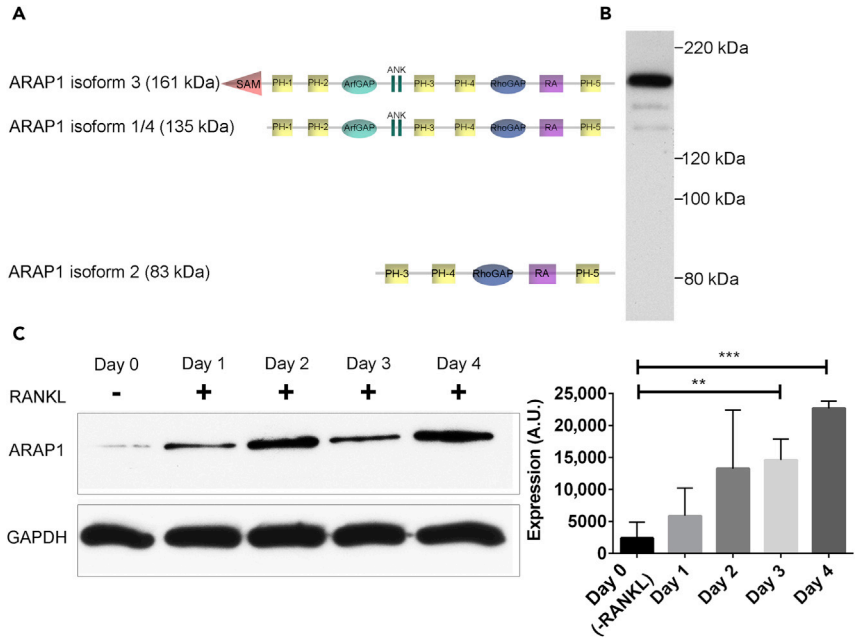

Figure 1. Expression of ARAP1 during Osteoclastogenesis

(A) Transcript variants of validated murine ARAP1 isoforms. The different domains are indicated. The target sequence of the stealth siRNA and AB, the epitope recognized by the anti-murine ARAP1 antibody, are situated at the C terminus of all isoforms.

(B) Immunoblotting of ARAP1 in osteoclasts.

(C) ARAP1 expression in osteoclasts and its precursors. RAW264.7 cells were grown on plastic in the absence or presence of RANKL and harvested at the indicated times. Undifferentiated RAW264.7 cells ("Day 0") were grown without RANKL, and cell extracts were prepared. Protein expression was determined by western blotting and quantified using the Fiji software. GAPDH was used as a control. The figures presented are representative of at least 3 independent experiments (mean ± SD; $^{**}p < 0.01$, $^{***}p < 0.001$).

See also Figure S1.

selectively recruited together with AP-3 onto membranes (Baust et al., 2008). Collectively, our analysis revealed that ARAP1 could regulate both actin dynamics and AP-3-dependent membrane traffic in osteoclasts.

ARAP1 Localization

Previous studies indicated a widespread localization of ARAP1 on different compartments of the biosynthetic and endocytic pathways as well as circular dorsal ruffles of cultured cells (Daniele et al., 2008; Miura et al., 2002; Hasegawa et al., 2012). In mature osteoclasts grown on glass or apatite-collagen-coated surfaces, endogenous ARAP1 localized to actin-rich podosomes and sealing zones as well as AP-3-coated compartments (Figure 2). The co-localization of ARAP1 with AP-3 was highly specific as indicated by the Pearson correlation of ~0.6 for both endogenous and overexpressed ARAP1 (Figure 2G). AP-3-positive structures also showed strong co-localization with an early endosome marker (EEA1) or VPS35, a subunit of the retromer complex found on early endosomes, but to a lesser extent with Rab7a, a late endosomal maker, and GM-130, a Golgi marker (Figures 2H and S2) (Dell'Angelica et al., 1997; Le Borgne et al., 1998). Thus, part of ARAP1 is present on AP-3-coated early endosomes, which also contain a large amount of the lysosomal membrane protein LAMP1 in osteoclasts (Figures 2B, 2F, and S2). ARAP1 localization would therefore be consistent with our MS-based proteomic analysis of ARAP1 interactors.

We also expressed a GFP-tagged ARAP1 isoform 3 in osteoclasts using a recombinant adenovirus. Expressed GFP-ARAP1 isoform 3 also localized to podosomes and sealing zones as well as to AP3-coated structures (Figures 2D and 2E). Interestingly, osteoclasts overexpressing GFP-ARAP1 isoform 3 had remarkably enlarged vesicles coated with AP-3 (Figures 2D, 2E, and S3). This phenomenon could be especially appreciated on glass, where osteoclasts are flat and large (Figure S3). The influence of ARAP1

Description	Alternative Names	Protein Molecular Weight (Da)	Exclusive Unique Peptide Count	Exclusive Unique Spectrum Count	Percentage Sequence Coverage (%)
SH3 domain-containing kinase-binding protein 1 isoform 1	CIN85	73,330.3	9	10	23.20%
		73,330.3	25	29	57.60%
F-actin-capping protein subunit beta isoform d	F-actin-capping protein	29,296.1	13	17	63.80%
		29,296.1	11	12	47.70%
F-actin-capping protein subunit alpha-1	F-actin-capping protein	32,751.7	8	9	51.00%
		32,751.7	7	8	54.50%
F-actin-capping protein subunit alpha-2	F-actin-capping protein	32,967.2	12	12	46.90%
		32,967.2	8	9	50.30%
mCG21234; isoform CRA_b	Filamin-α	280,463.8	46	48	26.90%
		280,463.8	2	2	1.21%
Gelsolin isoform X2	Gelsolin	88,212.5	3	3	5.24%
		88,212.5	13	13	22.80%
CD2-associated protein	METS-1	70,434.6	4	4	8.16%
		70,434.6	22	23	43.20%
Actin-related protein 3	ARP3	47,357.7	20	25	64.10%
		47,357.7	3	3	88.50%
Actin-related protein 2/3 complex subunit 3	ARP2/3 subunit3	20,525.9	2	2	22.50%
Actin-related protein 2/3 complex subunit 1B	ARP2/3 subunit 1B	41,063.6	12	15	39.80%
		41,063.6	2	2	6.18%
Actin-related protein 2/3 complex subunit 2	ARP2/3 subunit 3	34,357.8	11	14	43.00%
		34,357.8	2	2	7.33%
Proline-serine-threonine phosphatase-interacting protein 1	PSTPIP1	47,576.4	5	5	17.30%
		47,576.4	5	5	16.40%
Pstpip2 protein	PSTPIP2	39,020.7	4	4	22.20%
AP-3 complex subunit mu-1	AP-3μ1	46,937	16	26	53.60%
		46,937	14	16	58.10%
Adaptor-related protein complex 3; sigma 2 subunit	AP-3σ2	22,017.8	5	6	27.50%
		22,017.8	2	2	98.54%
Adaptor-related protein complex 3; beta 1 subunit; isoform CRA_b	AP-3β1	122,872.4	23	26	25.70%
		122,872.4	17	17	20.40%
AP-3 complex subunit delta-1	AP-3ɗ1	135,085.1	11	11	13.50%
		135,085.1	25	28	26.70%

Table 1. Putative ARAP1 Interactors Identified by Quantitative LC-MS/MS

(Continued on next page)

Description	Alternative Names	Protein Molecular Weight (Da)	Exclusive Unique Peptide Count	Exclusive Unique Spectrum Count	Percentage Sequence Coverage (%)
Vacuolar protein sorting-associated protein 13C	VPS13C	417,316.3	50	52	19.60%
		417,316.3	24	24	8.64%
Vacuolar protein sorting-associated protein 13A	Chorein, VPS13A	359,406	3	3	1.52%
		359,406	2	2	0.85%

Table 1. Continued

Anti-ARAP1-IgG-magnetic beads were mixed with an osteoclast lysate to purify endogenous ARAP1 and its interactors. After washing, the bound proteins were identified by LC-MS/MS. In this table putative interactors identified were illustrated.

overexpression on the morphology of AP-3-positive structures suggests that ARAP1 may regulate AP-3-dependent trafficking and/or endosome maturation.

ARAP1 Regulates Sealing Zone Dynamics and the Resorption Activity of Osteoclasts

We first followed by time-lapse video microscopy ARAP1 dynamics at individual podosomes using total internal reflection fluorescence microscopy and sealing zones labeled with the monomeric red fluorescent protein (mRFP)-tagged actin-binding domain of ezrin (mRFP-ABDE) expressed with a recombinant adenovirus. Figure S1 shows that ARAP1 dynamics follows that of actin at podosomal cores (Figures S1B and S1C and Video S1) and sealing zones (Video S2), indicating that ARAP1 remains associated with these actin-rich structures during their lifetime. We then performed small interfering RNA (siRNA)-mediated knockdown of ARAP1 isoforms using siRNAs targeting the C-terminal end of ARAP1 conserved in all murine transcript variants. Upon ARAP1 knockdown (90% efficiency), the podosomal belt normally observed at the periphery of osteoclasts grown on glass was disrupted. Podosomes had an abnormal podosome organization as they appeared more dispersed forming arbitrary clouds and rings (Figures 3A and 3D). When grown on apatite-collagen-coated surfaces, the osteoclasts assemble classical sealing zones, which are dynamic structures as observed by time-lapse video microscopy (Figure 3, Video S3). Upon ARAP1 depletion, siRNA-treated osteoclasts could only assemble very small sealing zone remnants (Figures 4A and 4B) whose dynamics was drastically reduced (Figure 4B and Video S4). These sealing zone remnants remained very static, unable to further assemble or disassemble (Figure 4B). Moreover, ARAP1-depleted osteoclasts were unable to resorb collagen/apatite-coated surfaces (Figure 4C). Remarkably, this phenotype could be rescued upon re-expression of the GFP-ARAP1 isoform 2, which lacks the ArfGAP domain (Figures 3B and 3C). Collectively, these results demonstrate that ARAP1 is a key component of podosomes, which regulates their assembly and dynamics to form sealing zones required for efficient degradation of bone-mimicking surfaces. Furthermore, our results indicate that only the RhoGAP domain of ARAP1 may regulate podosome/sealing dynamics.

ARAP1 Regulates AP-3 Coat Binding to Membranes and Trafficking of Lysosomal Membrane Proteins to the Ruffled Border

Our study shows that ARAP1 interacts with the AP-3 complex, a coat component required for the proper targeting of selected lysosomal membrane proteins to the endocytic system of every cell type. The Arf1 GTPase regulates AP-3 binding to membranes of early endosomes (Ooi et al., 1998). Therefore, it could be postulated that ARAP1 regulates Arf1 binding to membranes and consequently AP-3 recruitment onto membranes and the trafficking of lysosomal membrane proteins in osteoclasts. To test this hypothesis, we used an siRNA-based approach to inactivate ARAP1 and monitored the interaction of AP-3 with early endosomal membranes and the targeting of lysosomal membrane proteins in mature osteoclasts.

We first determined the amount of AP-3 bound to membranes by simply measuring the fluorescence intensities after labeling osteoclasts with anti-AP-3 antibodies. Remarkably, the knockdown of ARAP1 induced a 3-fold increase in the fluorescence intensity of membrane-bound AP-3 when compared with mock-treated osteoclasts (Figures 5A, 5B, and 5G). Moreover, the lysosomal membrane protein LAMP1 and Rab7a, which are markers of the ruffled border of osteoclasts grown on collagen-apatite-coated surfaces (Figures 5C, 5D, and S5) were barely detectable at the inner part of the sealing zone remnants after ARAP1 knockdown,

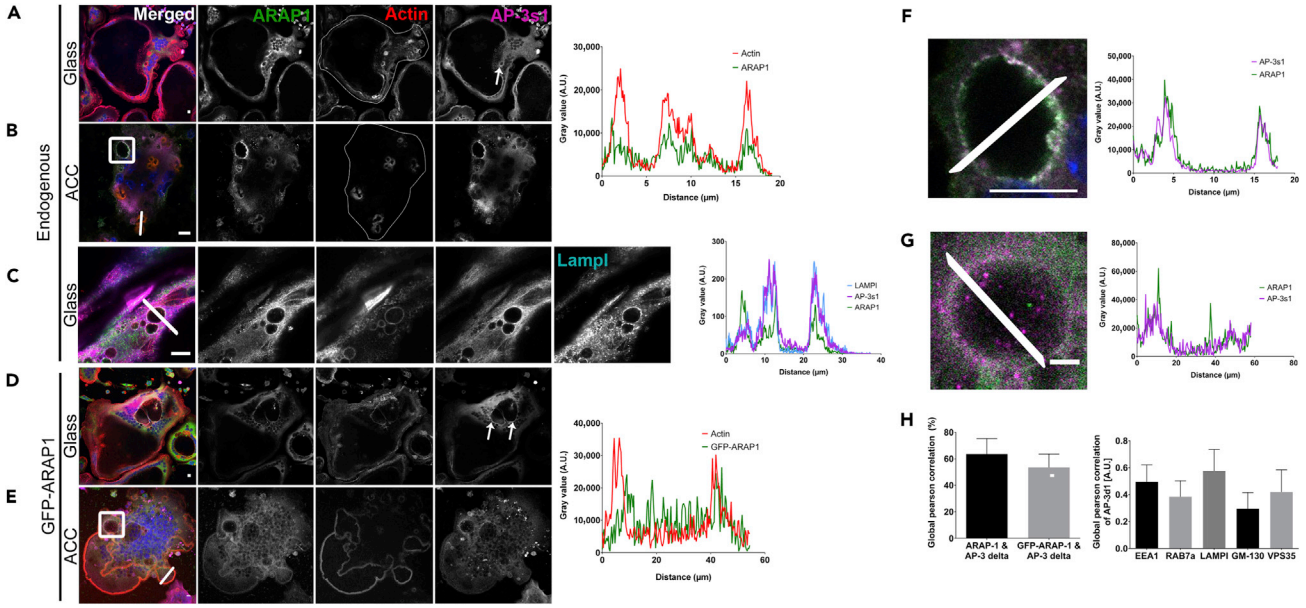

Figure 2. Localization of Endogenous and GFP-Tagged ARAP1 in Osteoclasts

(A–E) Osteoclasts were grown on glass or apatite-collagen-coated surfaces (ACCs), fixed, and stained for (A, B, D, and E) ARAP1 (green) and AP-3 (magenta) actin (red) and DAPI (blue) and (C) AP-3s1 (blue), actin (magenta), ARAP1 (red), and LAMPI (green). White arrows are pointing towards AP-3 positive endosomes. Outlines of single osteoclasts are depicted by white circles in the actin channel. Scale bar: 10 μm.

(F) Enlargement of rectangle in B. Fluorescence intensities across the indicated white lines (at sealing zones) were plotted. Images were analyzed using the Fiji software. Scale bar: 10 μm.

(G) Enlargement of rectangle in E. Fluorescence intensities across the white lines (at sealing zones) as indicated were plotted. Images were analyzed using the Fiji software. Scale bar: 10 μm.

(H) Descriptive statistics to identify ARAP1/AP-3-positive endosomes. The global Pearson correlation coefficients for endogenous and overexpressed ARAP1, AP-3δ, EEA1, Rab7a, LAMPI, GM-130, and VPS35 were determined using the Volocity software with automated thresholding (Costes et al., 2004). (n = 3, mean ± SD).

See also Figure S2.

indicating the absence of a ruffled border. These results suggest that in the absence of ARAP1 more AP-3 binds to early endosomal membranes and retains lysosomal membrane proteins in the endocytic system.

Our previous studies have shown that AP-3-dependent cargos like the lysosomal membrane protein LAMP1 are directed to the cell surface in the absence of AP-3, which results in a longer half-life of these proteins and their apparent accumulation in cells (Baust et al., 2008; Traikov et al., 2014). Therefore, we depleted osteoclasts from AP-3 using siRNAs targeting its μ subunit. When compared with control osteoclasts, AP-3μ-depleted osteoclasts were strongly enriched in LAMPI and LAMPII (a 4- and 2-fold increase, respectively) at the ruffled border (Figures 5H and S4). In addition, we found by western blotting more LAMPI in osteoclasts depleted of AP-3μ or ARAP1 than in control osteoclasts (Figure 5I). Thus, the ruffled border of AP-3-depleted osteoclasts is enriched in AP-3-dependent cargos, although AP-3μ knockdown had per se no effect on the organization of podosomes and sealing zones (Figures 4A and 4B). In addition, AP-3-depleted osteoclasts grown on collagen-apatite-coated surfaces exhibited a higher capacity to resorb the bone-mimicking surfaces that control osteoclasts (Figure 4D) Thus, AP-3, like ARAP1, controls the membrane composition of the ruffled border of osteoclasts and their capacity of digesting bone.

AP-3-Deficient Mice Are Osteoporotic

The results described above strongly suggest that AP-3-deficient mice should develop osteoporosis due to a higher activity of their osteoclasts to digest bone. To test this hypothesis, we examine the bone phenotype of mocha mice, a mouse model for the human Hermansky-Pudlak storage pool syndrome, which lack a functional AP-3 coat due to mutations in their δ subunit (Kantheti et al., 1998). Homozygous AP-3-depleted mice are extremely difficult to obtain because they die during early development and also during embryogenesis. Therefore, we decided to examine wild-type, heterozygous and homozygous animals from the

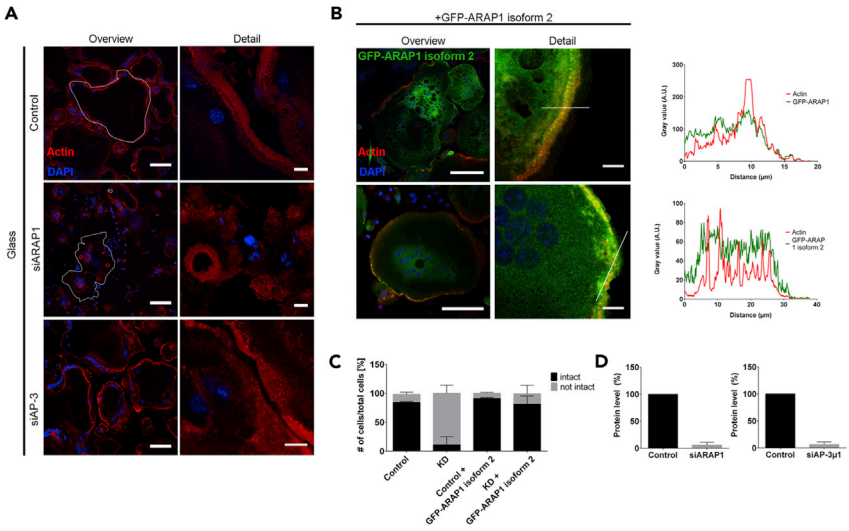

Figure 3. ARAP1 Affects Podosomal Belt Organization

(A) Effect of ARAP1 and AP-3 knockdown on podosomes in overview (scale bar: 100 µm) and detail (scale bar: 10 µm). (A) ARAP1 and AP-3 were depleted in osteoclast using stealth siRNA as described. Cells were fixed and stained on glass coverslips for DAPI (blue) and phalloidin (red). The outline of single osteoclasts were marked in white. Scale bar in overview: 100 µm; scale bar in detail: 10 µm.

(B) ARAP1 knockdown cells were subsequently transfected with GFP-tagged ARAP1 isoform 2 (green) using a recombinant adenovirus. Fluorescence intensities across the white lines (at podosomes) as indicated were plotted. Scale bar in overview: 100 µm; scale bar in detail: 10 µm.

(C) The number of osteoclasts in A and B with an intact and altered (not intact) podosomal belt were counted on an 11-mm glass coverslip and plotted. The intactness of the podosomal belt was judged based on the presence of a clear belt on the periphery of an osteoclast. If osteoclasts had dispersed podosomes or arbitrary rings that were phalloidin-positive within the cell, they were judged as non-intact. (n = 3, mean ± SD).

(D) The knockdown efficiencies were assessed by immunoblotting (ARAP1) or by qPCR (AP-3) and plotted. (mean ± SD).

same litters. We could collect 4 homozygous, 8 wild-type, and 11 heterozygous animals aged between 4 and 6 weeks. Tibias from these animals were collected and analyzed by micro X-ray computed tomography for trabecular bone volume, trabecular separation, trabecular number, and thickness. All these bone parameters were significantly lower in heterozygous and homozygous animals when compared with the wild-type, whereas trabecular separation significantly increased (Figures 6A–6D). This osteoporotic phenotype is in agreement with our *in vitro* bone digestion studies (Figure 4C) and further illustrates the importance of AP-3 in osteoclast function (Figure 6E).

DISCUSSION

Our study illustrates the functional importance of ARAP1 as a bridging factor coordinating podosome/sealing zone assembly and ruffled border biogenesis in osteoclasts. The ARAP1 Rho GAP domain may control Rho signaling for actin and sealing zone dynamics. ARAP1, most likely through its ArfGAP domain, controls the Arf-1-dependent association of AP-3 with membranes and consequently the delivery of lysosomal membrane proteins to the ruffled border. Alteration of any of these two coordinated processes affects the capacity of osteoclasts to digest bone.

ARAP1 is present at podosomes and sealing zones where it regulates their dynamics. How is ARAP1 recruited at this location? First, ARAP1 contains five PH domains able to bind to several phosphatidylinositol phosphates (PtdIns) (Campa et al., 2009). The first and third PH domains fit the consensus for binding phosphatidylinositol-3,4,5-trisphosphate [PtdIns(3,4,5)P_3] (Daniele et al., 2008; Miura et al., 2002), a phospholipid whose synthesis is activated at the plasma membrane upon integrin binding to extracellular, RGD motif-containing proteins (Yu et al., 2013). In addition, PtdIns(3,4,5)P_3 binding to the PH domain stimulates ARAP1 GAP activity (Campa et al., 2009). However, these PH domains exhibit a low affinity for PtdIns(3,4,5)P_3. Therefore ARAP1 at podosomes must be stabilized by interactions with other podosomal components. Our quantitative proteomics analysis of the ARAP1 interactome clearly shows that ARAP1 interacts with the

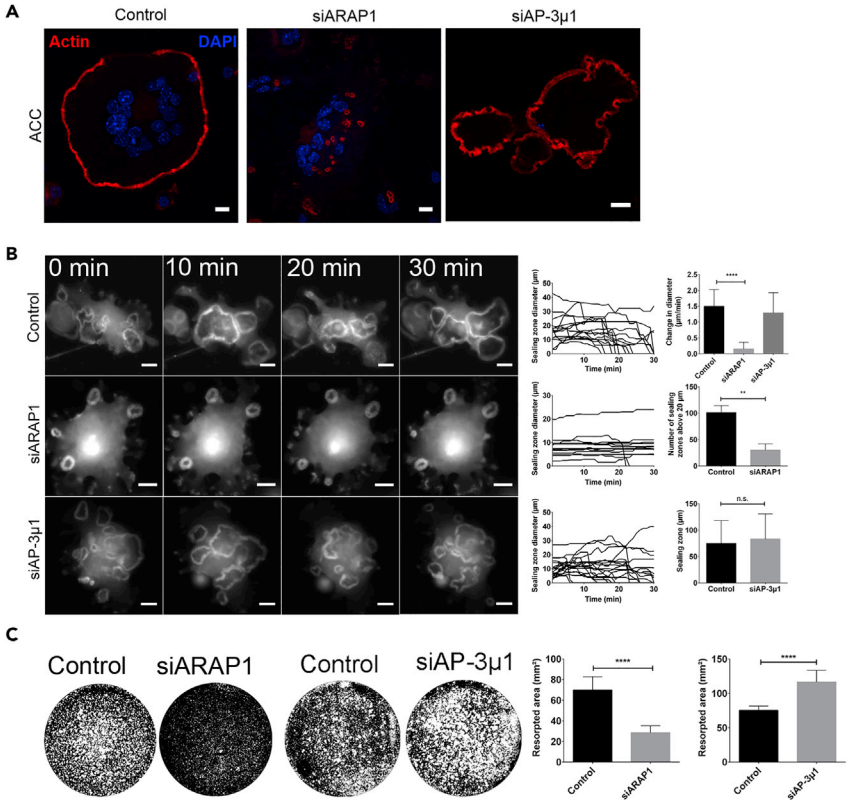

Figure 4. ARAP1 and AP-3 Depletion Affects Osteoclast Resorption

(A) Effect of siRNA-mediated ARAP1 depletion on the podosomal belt and sealing zones. Osteoclasts were treated with siRNA targeting the ARAP1 genes or mock siRNA and then grown for 48 hr on osteological disks as indicated in Methods. Cells were then fixed and stained with phalloidin (red) and DAPI (blue). (Scale bar: 10 µm). The knockdown efficiency was determined by western blot. The number of osteoclasts with intact and altered (not intact) podosomal belts was counted on an 11-mm glass coverslip and plotted.

(B) Effect of siRNA-mediated ARAP1 and AP-3µ1 depletion on sealing zone dynamics. Osteoclasts were treated with siRNAs targeting the corresponding genes or mock siRNA and then plated on apatite-collagen-coated (ACC) multiwell dishes. After 24 hr, they were infected with a recombinant adenovirus encoding the mRFP-ezrin actin-binding domain. After 32 hr, osteoclasts were imaged by time-lapse microscopy (200 ms per frame, 1 frame per minute for 30 min, scale bar: 10 µm). See also Videos S3, S4, and S5. Sealing zone diameter was measured using the Fiji software. The relative sealing zone diameter was plotted for each sealing zone assessed. The change of the sealing zone diameter per minute was plotted and tested using Student's t test. (n = 3, mean ± SD; ****$p < 0.0001$) The size of the sealing zones above 20 µm in control and siARAP1- and siAP-3-treated osteoclasts was counted on an 11-mm ACC-coated glass coverslip (n = 3, mean ± SD; **$p < 0.01$). The knockdown efficacy of AP-3µ1 was determined with qPCR.

(C) Effect of siRNA-mediated ARAP1 and AP-3µ1 depletion on resorption. The resorptive capacity of osteoclasts treated with siARAP1 or mock siRNA was measured using Corning Osteo Assay Surfaces. The resorbed area from siARAP1 and siAP-3µ1 osteoclasts on 24-well Osteo Assay dishes was plotted using Student's t test. (n = 3, mean ± SD; ****$p < 0.0001$).

scaffolding BAR-domain PSTPIP1/2, which regulates the assembly/disassembly of podosomes and sealing zones. This correlates well with our previous studies showing that ARAP1 is found in the PSTPIP1/2 interactome (Sztacho et al., 2016). PSTPIP1 interacts with the phosphotyrosine protein phosphatase PTPN6 through its BAR-domain and the phosphatidylinositol 5-phosphatase SHIP1/2 (Sztacho et al., 2016) through its SH3 domain. PTPN6 may also dephosphorylate other proteins that are in proximity to the membrane, such as Syk (Maeda et al., 1999). SHIP1 is specific for hematopoietic cells and keeps the levels of phosphatidylinositol (3,4,5)-trisphosphate ($PI(3,4,5)P_3$) low, a regulation that is involved in podosome disassembly (Muraille et al., 1999). Although not identified in the proteomic approach for ARAP1 interactors represented here, ARAP1 may also bind to SHIP1/2 via its SAM domain, similar to the ARAP3 isoform SAM domain, which binds to SHIP2 (Raaijmakers et al., 2007). We also identify as an ARAP1 interactor CIN85, also known as a SH3KBP1 (SH3 domain kinase-binding protein 1); Ruk (regulator of ubiquitous kinase);

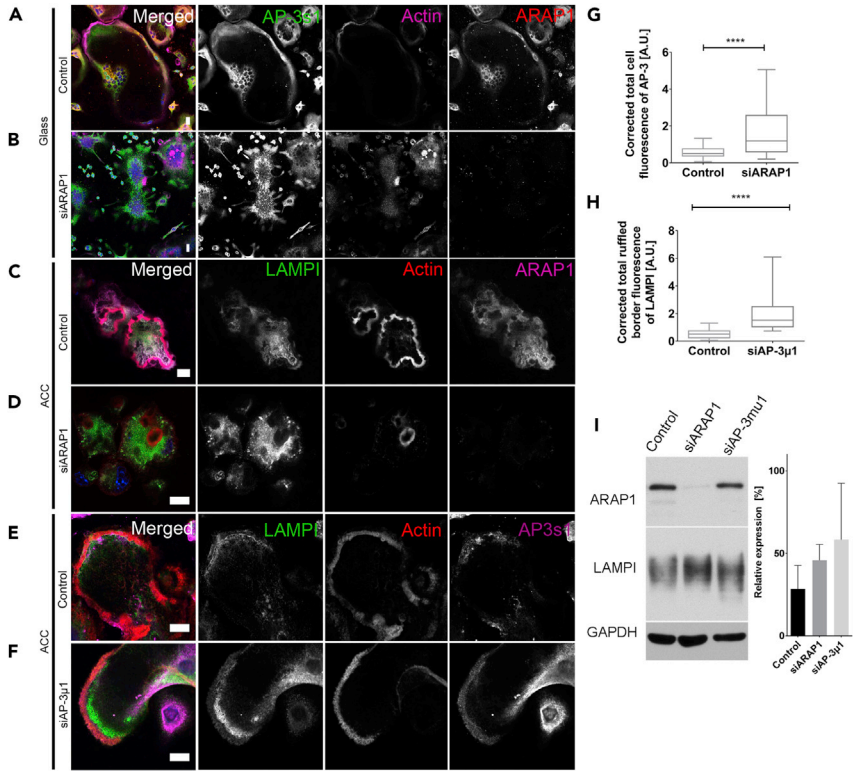

Figure 5. ARAP1 Regulates the Association of AP-3 with Membranes and LAMPI Trafficking to the Ruffled Border

(A–F) Effect of siRNA-mediated depletion of ARAP1 or AP-3µ1 on AP-3 and LAMPI fluorescent signals. Osteoclasts treated with siRNAs targeting ARAP1 or AP-3µ1 or mock siRNA were grown on glass or apatite-collagen-coated (ACC) coverslips, fixed, and stained with DAPI and phalloidin and with anti-ARAP1 or anti-AP-3s1 antibodies or anti-LAMP1 antibodies. (scale bar: 10 µm).

(G) AP-3s1 fluorescence intensities in siARAP1-treated osteoclasts were measured from individual stacks and relative values were plotted (n = 3, mean ± SD; ****$p < 0.0001$).

(H) The relative LAMPI fluorescence intensity at the ruffled border in AP-3µ1 knockdown (KD) was measured and plotted (n = 3, mean ± SD; Student's t test, ****$p < 0.0001$). The large error bars can be explained by variations in the KD efficiency in individual osteoclasts.

(I) Effect of siRNA-mediated depletion of ARAP1 and AP-3µ1 depletion on steady-state LAMPI. Osteoclasts treated with siARAP1, siAP-3µ1, or mock siRNA were grown on plastic, harvested, and immunoblotted with anti-LAMPI, ARAP1, and GAPDH antibodies. AP-3 knockdown efficiency was determined by qPCR. The intensity of LAMPI in immunoblotting was analyzed using the Fiji software and plotted.

and SETA (SH3 domain-containing gene expressed in tumorigenic astrocytes) (Narita et al., 2001; Gout et al., 2000; Bogler et al., 2000; Borinstein et al., 2000; Dikic, 2002). CIN85 also interacts with SHIP1 in B cells (Havrylov et al., 2009; Buchse et al., 2011). We therefore propose that ARAP1 is part of a large protein complex composed of PSTPIP1, PTPN6, SHIP1/2, and CIN85. This complex functions by combining local dephosphorylation of PI(3,4,5)P_3 lipids through SHIP1/2, dephosphorylation of Src-dependent podosomal substrates through PTPN6, and down-regulation of Rho signaling through ARAP1 to control podosome and sealing zone dynamics.

Our study strongly suggests that a down-regulation of Rho signaling is essential for maintaining the highly dynamic nature of podosomes and sealing zones. ARAP1 knockdown resulting in a higher Rho signaling disrupts podosomal belt organization and reduces the size and dynamics of sealing zones, thereby resulting in osteoclasts unable to resorb bone-mimicking surfaces. Re-expression of an ARAP1 isoform containing a Rho GAP domain but lacking the Arf domain is sufficient to restore podosome and sealing zone dynamics. We could not directly demonstrate that the Rho GAP activity is necessary for this function. This would have required the re-expression of an ARAP1 mutant impaired in its Rho GAP activity in osteoclasts depleted of endogenous ARAP1. Such experiments, as described here with ARAP1 isoform 2 (Figures 3B

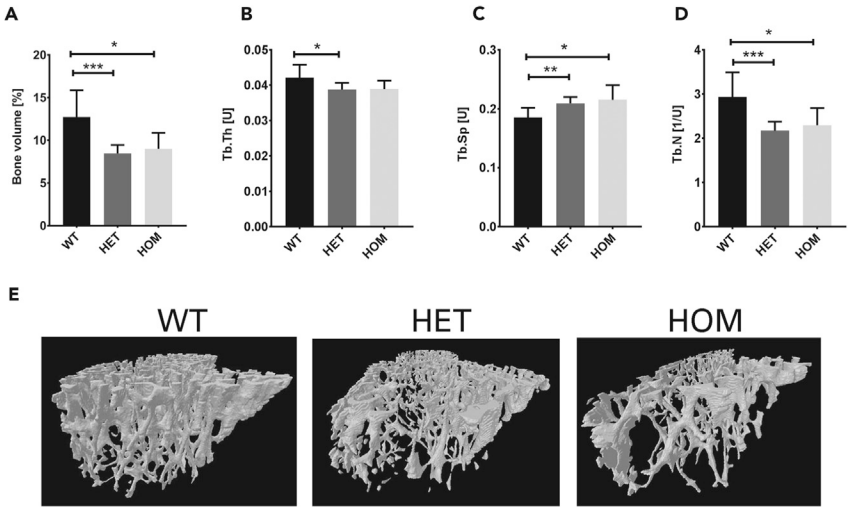

Figure 6. Bone Phenotype of Mocha Mice

(A–E) Mocha mice aged 4–6 weeks were analyzed for trabecular bone parameters at their right tibias. (A–D) Bone volume, trabecular thickness (Tb.Th.), trabecular separation (Tb.Sp.), and trabecular number were analyzed with the CTan and CTvol software after microCT. Statistical analysis was done in the GraphPad Prism 7 Software using ordinary one-way ANOVA (n = 8 [WT], 11 [HET], and 4 [HOM]; mean ± SD; *p < 0.05, **p < 0.01, ***p < 0.001). (E) 3D projections of the trabecular bone of *mocha* mice.

and 3C), are technically challenging due to the adenovirus-based re-expression system, which renders difficult the re-expression of large size proteins like ARAP1. Potential targets of the ARAP1 GAP activity are RhoA, Rac1, or Cdc42 (Miura et al., 2002; Destaing et al., 2003). RhoA signaling is required for osteoclast podosome organization, motility, and bone osteoclasts by activating integrin-dependent activation of phosphoinositide synthesis (Chellaiah et al., 2000). Cdc42 signaling is also necessary since its GEF FGD6 is required for podosome formation through the assembly of complexes comprising the Cdc42 interactor IQGAP1, the Rho GAP ARHGAP10, and the integrin interactors talin-1/2 or filamin A (Steenblock et al., 2014). Similarly, the Rac1 guanine exchange factor FARP2 is required for localized activation of GTP-bound Rac1 into podosome-ring-like structures, where it controls integrin β3 activity during osteoclastogenesis (Takegahara et al., 2010). Therefore, more work will be needed to identify the Rho GTPase down-regulated by ARAP1 and understand its precise role in controlling Rho signaling at podosomes and sealing zones.

ARAP1 is also present on early endosomes where it regulates the AP-3-dependent traffic of lysosomal membrane proteins to the ruffled border. ARAP1 interaction with early endosomes is first due to the presence of the PH 1, 2, 4, or 5 domain, which binds PtdIns(3)P (Daniele et al., 2008), a phospholipid enriched at the cytoplasmic surface of early endosomes (Peden et al., 2004), and second due to its interaction with the AP-3 complex, which is mostly present on this compartment. *In vitro,* the ARAP1 ArfGAP domain preferentially hydrolyzes Arf1-GTP (Miura et al., 2002; Ooi et al., 1998), which is required for efficient AP-3 binding to PtdIns(3)P-rich membranes (Nie et al., 2003). Accordingly, ARAP1–depleted osteoclasts exhibit a higher amount of AP-3 bound to their membranes, and the overexpression of ARAP1 in osteoclasts resulted in enlarged AP-3-coated endosomes, suggesting that endosome maturation is impaired. Thus, ARAP1, like AGAP1 binding to AP-3 δ and σ subunit (Nie et al., 2003), is one of the ArfGAPs regulating the Arf-1-dependent binding of AP-3 to early endosomes. We could not directly demonstrate that ArfGAP activity of ARAP1 is essential for this function for the same reasons as explained above for its Rho GAP activity. We have previously shown that in HeLa cells AP-3 mediates the intracellular targeting of lysosomal membrane proteins to late endocytic compartments and that in its absence lysosomal membrane proteins are allowed to have access to the cell surface (Traikov et al., 2014; Le Borgne et al., 1998). In osteoclasts, the ruffled border is a highly convoluted membrane enriched in lysosomal membrane proteins. We show here that lysosomal membrane proteins such as LAMP1 and LAMPII are more enriched at the ruffled border and early endosomes after AP-3 depletion. In contrast, we found no change in the secretion of β-hexosaminidase in ARAP1-depleted osteoclasts, a classical lysosomal enzyme whose targeting is AP-3 independent (data

not shown). It has been proposed that the ruffled border of osteoclasts results from the fusion of intracellular acidic vesicles, most likely lysosomes, with the ruffled border (Mulari et al., 2003). We propose that the regulation of AP-3 binding onto early endosomes by ARAP1 would modulate the access of newly synthesized lysosomal membrane proteins to the ruffled border of osteoclasts.

What is the consequence of modulating the protein content of the ruffled border? Clearly, our study shows that the activity of osteoclasts in bone resorption is affected. ARAP1-depleted osteoclasts are impaired in bone-mimicking surface digestion, most likely due to the lack of formation of a proper sealing zone and ruffled border. Strikingly, AP-3-depleted osteoclasts, which can still form normal sealing zones, are more active in surface resorption that controls osteoclasts. The most likely explanation is that the ruffled border is, as we show here, enriched in lysosomal membrane proteins and probably other proteins involved in bone digestion like the V-ATPase and chloride channels, making the resorption lacuna more efficient in degradation. Accordingly, AP-3δ-deficient *mocha* mice develop severe osteoporosis already at a relatively early age. *Mocha* mice provide a model of Hermansky-Pudlack storage pool syndrome. Hence, these mice are characterized by defective platelets, coat, and eye color as a consequence of defective sorting of AP-3-dependent cargo proteins to lysosomes and lysosome-related organelles of specialized cells such as melanosomes, platelet-dense granules, and neurotransmitter vesicles (Kantheti et al., 1998). Thus, our results would strongly suggest that patients with Hermansky-Pudlack storage pool syndrome also suffer from osteoporosis.

ARAP1 KO mice generated as part of the International Mouse Phenotyping Consortium show a bone phenotype as they have abnormally short tibias, thus indicating a key function of ARAP1 in bone biology (www.impc.org).

METHODS

All methods can be found in the accompanying Transparent Methods supplemental file.

SUPPLEMENTAL INFORMATION

Supplemental Information includes Transparent Methods, five figures, and five videos and can be found with this article online at https://doi.org/10.1016/j.isci.2018.07.019.

ACKNOWLEDGMENT

We thank the different lab members and Euroclast members especially Anh Nhi Tran and Sofia Traikov for their helpful discussions and critical comments. Dorothee Thiel and Theresia Pursche kindly provided their technical assistance. We would further like to acknowledge Kevin S. Mackenzie from the Microscopy Facility at the University of Aberdeen for technical assistance in the microCT studies. We would like to thank the Mass Spectrometry Facility at the MPI-CBG, Dresden, and the Light Microscopy Facility of BIOTEC at Technische Universität, Dresden, for their expertise. This work and S.S. were supported in part by the Marie Curie Initial Training Network (Euroclast, FP7-People-2013-ITN: #607447). B.H.'s research was also supported by TU Dresden (Program Support the Best) and the Deutsche Forschungsgemeinschaft (TRR 83/1-2014, HO 2584-10-1, HO 2584/9-1). T.G.'s group was funded by grants from Association Française contre les Myopathies (Research Grant 16612), the French National Research Agency (NeuroImmunoSynapse ANR-13-BSV2-0018-02, MetDePaDi ANR-16-CE16-0012), the Ecole des Neurosciences de Paris (ENP), the Fondation pour la Recherche Médicale (FRM), Who am I? Labex (Idex ANR-11-IDEX-0005-01), Prix Coup d'élan pour la recherche française of the Fondation Bettencourt Schueller, and awards of the Association Robert Debré pour la Recherche Médicale to T.G.

AUTHOR CONTRIBUTIONS

S.S. designed, performed, and analyzed the experiments. L.D. and T.G. provided the mocha mice. S.S. and B.H. designed and analyzed the experiments and wrote the manuscript.

DECLARATION OF INTERESTS

The authors declare no competing interests.

Received: March 21, 2018
Revised: June 6, 2018
Accepted: July 20, 2018
Published: August 31, 2018

REFERENCES

Akamine, A., Tsukuba, T., Kimura, R., Maeda, K., Tanaka, Y., Kato, K., and Yamamoto, K. (1993). Increased synthesis and specific localization of a major lysosomal membrane sialoglycoprotein (LGP107) at the ruffled border membrane of active osteoclasts. Histochemistry *100*, 101–108.

Baust, T., Anitei, M., Czupalla, C., Parshyna, I., Bourel, L., Thiele, C., Krause, E., and Hoflack, B. (2008). Protein networks supporting AP-3 function in targeting lysosomal membrane proteins. Mol. Biol. Cell *19*, 1942–1951.

Bogler, O., Furnari, F.B., Kindler-Roehrborn, A., Sykes, V.W., Yung, R., Huang, H.J., and Cavenee, W.K. (2000). SETA: a novel SH3 domain-containing adapter molecule associated with malignancy in astrocytes. Neuro Oncol. *2*, 6–15.

Borinstein, S.C., Hyatt, M.A., Sykes, V.W., Straub, R.E., Lipkowitz, S., Boulter, J., and Bogler, O. (2000). SETA is a multifunctional adapter protein with three SH3 domains that binds Grb2, Cbl, and the novel SB1 proteins. Cell. Signal. *12*, 769–779.

Buccione, R., Orth, J.D., and McNiven, M.A. (2004). Foot and mouth: podosomes, invadopodia and circular dorsal ruffles. Nat. Rev. Mol. Cell Biol. *5*, 647–657.

Buchse, T., Horras, N., Lenfert, E., Krystal, G., Körbel, S., Schümann, M., Krause, E., Mikkat, S., and Tiedge, M. (2011). CIN85 interacting proteins in B cells-specific role for SHIP-1. Mol. Cell. Proteomics *10*, M110.006239.

Campa, F., Yoon, H.-Y., Ha, V.L., Szentpetery, Z., Balla, T., and Randazzo, P.A. (2009). A PH domain in the Arf GTPase-activating protein (GAP) ARAP1 binds Phosphatidylinositiol 3,4,5-trisphosphate and regulates Arf GAP activity independently of recruitment to the plasma membranes. J. Biol. Chem. *284*, 28069–28083.

Chellaiah, M.A. (2005). Regulation of actin ring formation by Rho GTPases in osteoclasts. J. Biol. Chem. *280*, 32930–32943.

Chellaiah, M.A., Soga, N., Swanson, S., Mcallister, S., Alvarez, U., Wang, D.M., Dowdy, S.F., and Hruska, K.A. (2000). Rho-A is critical for osteoclast podosome organization, motility, and bone resorption. J. Biol. Chem. *275*, 11993–12002.

Costes, S.V., Daelemans, D., Cho, E.H., Dobbin, Z., Pavlakis, G., and Lockett, S. (2004). Automatic and quantitative measurement of protein–protein colocalization in live cells. Biophys. J. *86*, 3993–4003.

Czupalla, C., Mansukoski, H., Pursche, T., Krause, E., and Hoflack, B. (2005). Comparative study of protein and mRNA expression during osteoclastogenesis. Proteomics *5*, 3868–3875.

Daniele, T., Di Tullio, G., Santoro, M., Turacchio, G., and De Matteis, M.A. (2008). ARAP1 regulates EGF receptor trafficking and signalling. Traffic *9*, 2221–2235.

Dell'Angelica, E.C., Ohno, H., Ooi, C.E., Rabinovich, E., Roche, K.W., and Bonifacino, J.S. (1997). AP-3: an adaptor-like protein complex with ubiquitous expression. EMBO J. *16*, 917–928.

Destaing, O., Saltel, F., Geminard, J.C., Jurdic, P., and Bard, F. (2003). Podosomes display actin turnover and dynamic self-organization in osteoclasts expressing actin-green fluorescent protein. Mol. Biol. Cell *14*, 407–416.

Dikic, I. (2002). CIN85/CMS family of adaptor molecules. FEBS Lett. *529*, 110–115.

Gout, I., Middleton, G., Adu, J., Ninkina, N.N., Drobot, L.B., Filonenko, V., Matsuka, G., Davies, A.M., Waterfield, M., and Buchman, V.L. (2000). Negative regulation of PI 3-kinase by Ruk, a novel adaptor protein. EMBO J. *19*, 4015–4025.

Hasegawa, J., Tsujita, K., Takenawa, T., and Itoh, T. (2012). ARAP1 regulates the ring size of circular dorsal ruffles through Arf1 and Arf5. Mol. Biol. Cell *23*, 2481–2489.

Havrylov, S., Rzhepetskyy, Y., Malinowska, A., Drobot, L., and Redowicz, M.J. (2009). Proteins recruited by SH3 domains of Ruk/CIN85 adaptor identified by LC-MS/MS. Proteome Sci. *7*, 21.

Heckel, T., Czupalla, C., Expirto Santo, A.I., Anitei, M., Arantzazu Sanchez-Fernandez, M., Mosch, K., Krause, E., and Hoflack, B. (2009). Src-dependent repression of ARF6 is required to maintain podosome-rich sealing zones in bone-digesting osteoclasts. Proc. Natl. Acad. Sci. USA *106*, 1451–1456.

Kantheti, P., Qiao, X., Diaz, M.E., Peden, A.A., Meyer, G.E., Carskadon, S.L., Kapfhamer, D., Sufalko, D., Robinson, M.S., Noebels, J.L., and Burmeister, M. (1998). Mutation in AP-3 delta in the mocha mouse links endosomal transport to storage deficiency in platelets, melanosomes, and synaptic vesicles. Neuron *21*, 111–122.

Le Borgne, R., Alconada, A., Bauer, U., and Hoflack, B. (1998). The mammalian AP-3 adaptor-like complex mediates the intracellular transport of lysosomal membrane glycoproteins. J. Biol. Chem. *273*, 29451–29461.

Linder, S., and Aepfelbacher, M. (2003). Podosomes: adhesion hot-spots of invasive cells. Trends Cell Biol. *13*, 376–385.

Maeda, A., Scharenberg, A.M., Tsukada, S., Bolen, J.B., Kinet, J.P., and Kurosaki, T. (1999). Paired immunoglobulin-like receptor B (PIR-B) inhibits BCR-induced activation of Syk and Btk by SHP-1. Oncogene *18*, 2291–2297.

Miura, K., Jacques, K.M., Stauffer, S., Kubosaki, A., Zhu, K.J., Hirsch, D.S., Resau, J., Zheng, Y., and Randazzo, P.A. (2002). ARAP1: a point of convergence for Arf and Rho signaling. Mol. Cell *9*, 109–119.

Mulari, M., Vaaraniemi, J., and Vaananen, H.K. (2003). Intracellular membrane trafficking in bone resorbing osteoclasts. Microsc. Res. Tech. *61*, 496–503.

Muraille, E., Pesesse, X., Kuntz, C., and Erneux, C. (1999). Distribution of the src-homology-2-domain-containing inositol 5-phosphatase SHIP-2 in both non-haemopoietic and haemopoietic cells and possible involvement of SHIP-2 in negative signalling of B-cells. Biochem. J. *342* (Pt 3), 697–705.

Narita, T., Amano, F., Yoshizaki, K., Nishimoto, N., Nishimura, T., Tajima, T., Namiki, H., and Taniyama, T. (2001). Assignment of SH3KBP1 to human chromosome band Xp22.1–>p21.3 by in situ hybridization. Cytogenet. Cell Genet. *93*, 133–134.

Nie, Z.Z., Boehm, M., Boja, E.S., Vass, W.C., Bonifacino, J.S., Fales, H.M., and Randazzo, P.A. (2003). Specific regulation of the adaptor protein complex AP-3 by the Arf GAP AGAP1. Dev. Cell *5*, 513–521.

Ooi, C.E., Dell'Angelica, E.C., and Bonifacino, J.S. (1998). ADP-Ribosylation factor 1 (ARF1) regulates recruitment of the AP-3 adaptor complex to membranes. J. Cell Biol. *142*, 391–402.

Palokangas, H., Mulari, M., and Vaananen, H.K. (1997). Endocytic pathway from the basal plasma membrane to the ruffled border membrane in bone-resorbing osteoclasts. J. Cell Sci. *110* (Pt 15), 1767–1780.

Peden, A.A., Oorschot, V., Hesser, B.A., Austin, C.D., Scheller, R.H., and Klumperman, J. (2004). Localization of the AP-3 adaptor complex defines a novel endosomal exit site for lysosomal membrane proteins. J. Cell Biol. *164*, 1065–1076.

Raaijmakers, J.H., Deneubourg, L., Rehmann, H., De Koning, J., Zhang, Z., Krugmann, S., Erneux, C., and Bos, J.L. (2007). The PI3K effector Arap3 interacts with the PI(3,4,5)P3 phosphatase SHIP2 in a SAM domain-dependent manner. Cell. Signal. *19*, 1249–1257.

Saltel, F., Destaing, O., Bard, F., Eichert, D., and Jurdic, P. (2004). Apatite-mediated actin dynamics in resorbing osteoclasts. Mol. Biol. Cell *15*, 5231–5241.

Soriano, P., Montgomery, C., Geske, R., and Bradley, A. (1991). Targeted disruption of the c-src proto-oncogene leads to osteopetrosis in mice. Cell *64*, 693–702.

Steenblock, C., Heckel, T., Czupalla, C., Espirito Santo, A.I., Niehage, C., Sztacho, M., and Hoflack, B. (2014). The Cdc42 guanine nucleotide exchange factor FGD6 coordinates cell polarity and endosomal membrane

recycling in osteoclasts. J. Biol. Chem. *289*, 18347–18359.

Sztacho, M., Segeletz, S., Sanchez-Fernandez, M.A., Czupalla, C., Niehage, C., and Hoflack, B. (2016). BAR proteins PSTPIP1/2 regulate podosome dynamics and the resorption activity of osteoclasts. PLoS One *11*, e0164829.

Takegahara, N., Kang, S., Nojima, S., Takamatsu, H., Okuno, T., Kikutani, H., Toyofuku, T., and Kumanogoh, A. (2010). Integral roles of a guanine nucleotide exchange factor, FARP2, in osteoclast podosome rearrangements. FASEB J. *24*, 4782–4792.

Teitelbaum, S.L. (2000). Bone resorption by osteoclasts. Science *289*, 1504–1508.

Traikov, S., Stange, C., Wassmer, T., Paul-Gilloteaux, P., Salamero, J., Raposo, G., and Hoflack, B. (2014). Septin6 and Septin7 GTP binding proteins regulate AP-3- and ESCRT-dependent multivesicular body biogenesis. PLoS One *9*, e109372.

Vaananen, H.K., Karhukorpi, E.K., Sundquist, K., Wallmark, B., Roininen, I., Hentunen, T., Tuukkanen, J., and Lakkakorpi, P. (1990). Evidence for the presence of a proton pump of the vacuolar H(+)-ATPase type in the ruffled borders of osteoclasts. J. Cell Biol. *111*, 1305–1311.

van Meel, E., Boonen, M., Zhao, H., Oorschot, V., Ross, F.P., Kornfeld, S., and Klumperman, J. (2011). Disruption of the Man-6-P targeting pathway in mice impairs osteoclast secretory lysosome biogenesis. Traffic *12*, 912–924.

Yoon, H.-Y., Kales, S.C., Luo, R., Lipkowitz, S., and Randazzo, P.A. (2011). ARAP1 association with CIN85 affects epidermal growth factor receptor endocytic trafficking. Biol. Cell *103*, 171–184.

Yu, C.H., Rafiq, N.B., Krishnasamy, A., Hartman, K.L., Jones, G.E., Bershadsky, A.D., and Sheetz, M.P. (2013). Integrin-matrix clusters form podosome-like adhesions in the absence of traction forces. Cell Rep. *5*, 1456–1468.

Zhao, H., Ettala, O., and Vaananen, H.K. (2002). Intracellular membrane trafficking pathways in bone-resorbing osteoclasts revealed by cloning and subcellular localization studies of small GTP-binding rab proteins. Biochem. Biophys. Res. Commun. *293*, 1060–1065.

ISCI, Volume *6*

Supplemental Information

ARAP1 Bridges Actin Dynamics and AP-3-Dependent Membrane Traffic in Bone-Digesting Osteoclasts

Sandra Segeletz, Lydia Danglot, Thierry Galli, and Bernard Hoflack

Supplementary information

Supplemental figures.

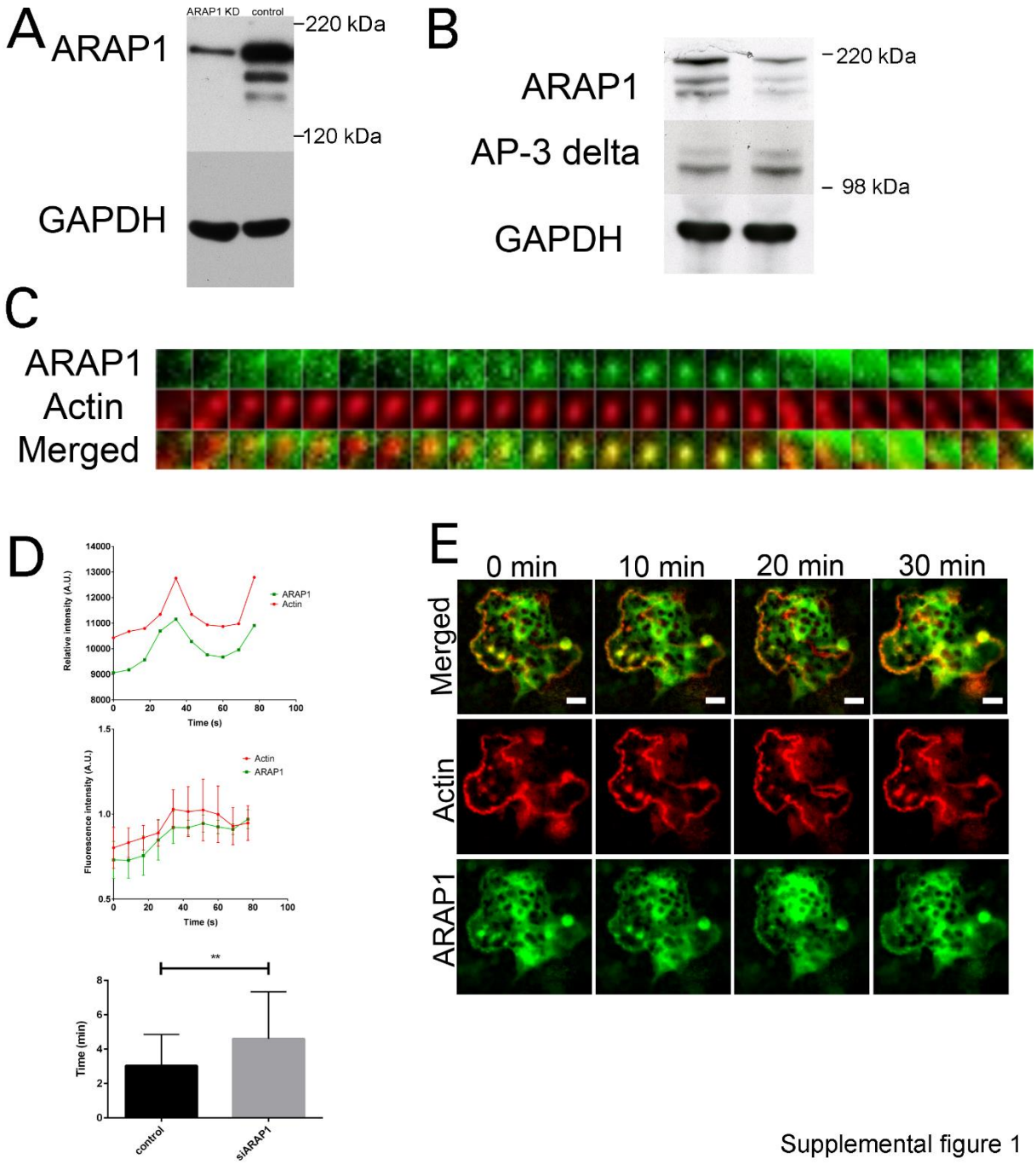

Supplemental figure 1

Figure S1. Dynamic behavior of ARAP1 and actin on podosomes and sealing zones. Related to Figure 1 and 2

A) ARAP1 depleted osteoclasts were analyzed for ARAP1 expression using immunoblotting. Osteoclasts were grown either on glass or on ACC coated dishes and transfected with constructs to express GFP-ARAP1 and mRFP-tagged actin-binding domain of Ezrin (mRFP-ABDE). The sealing zones were observed with time-lapse videomicroscopy 48 hours after transfection (200 msec. per frame, 1 frame per 1 min. for 30 min). **B-C)** Individual podosomes were observed with total internal reflection time-lapse videomicroscopy 48 hours post transfection (100 msec. per frame, 1 frame per 2 sec), see Movie 1. There fluorescence

intensity was plotted vs. time. **D)** The colocalization of sealing zones with ARAP1 was observed using time-laps videomicroscopy (200 msec. per frame, 1 frame per 1 min. for 30 min). See Movie 2.

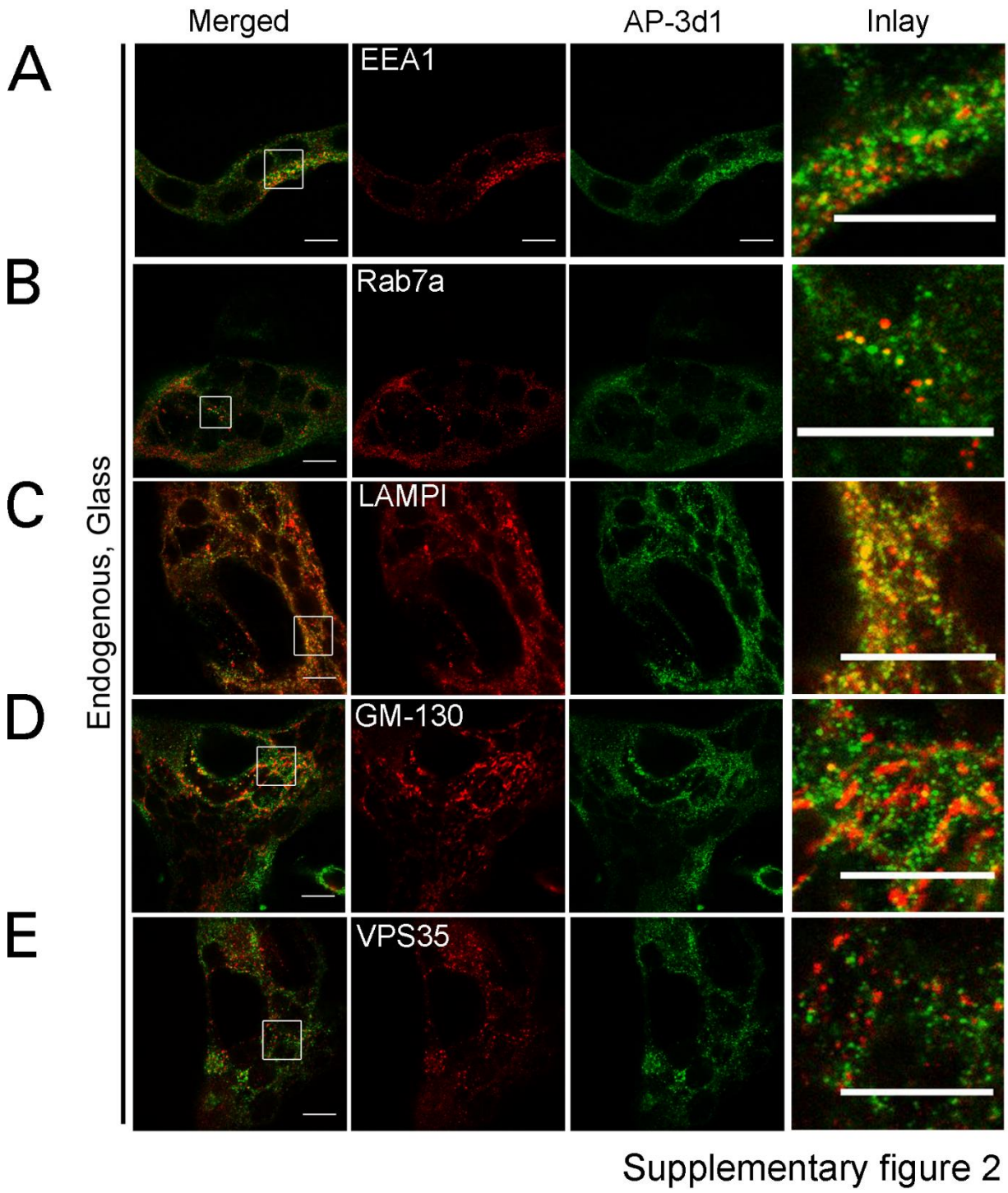

Figure S2. AP-3 characterization in osteoclasts. Related to Figure 2.

(A-E) Characterization of AP-3 positive endosomes in osteoclasts. Osteoclasts were grown on glass, fixed and stained with AP-3d1 (green), actin (magenta), DAPI (blue) and different markers of the endocytic pathway EEA1, Rab7a, LAMPI, GM-130, VPS35 (all red).

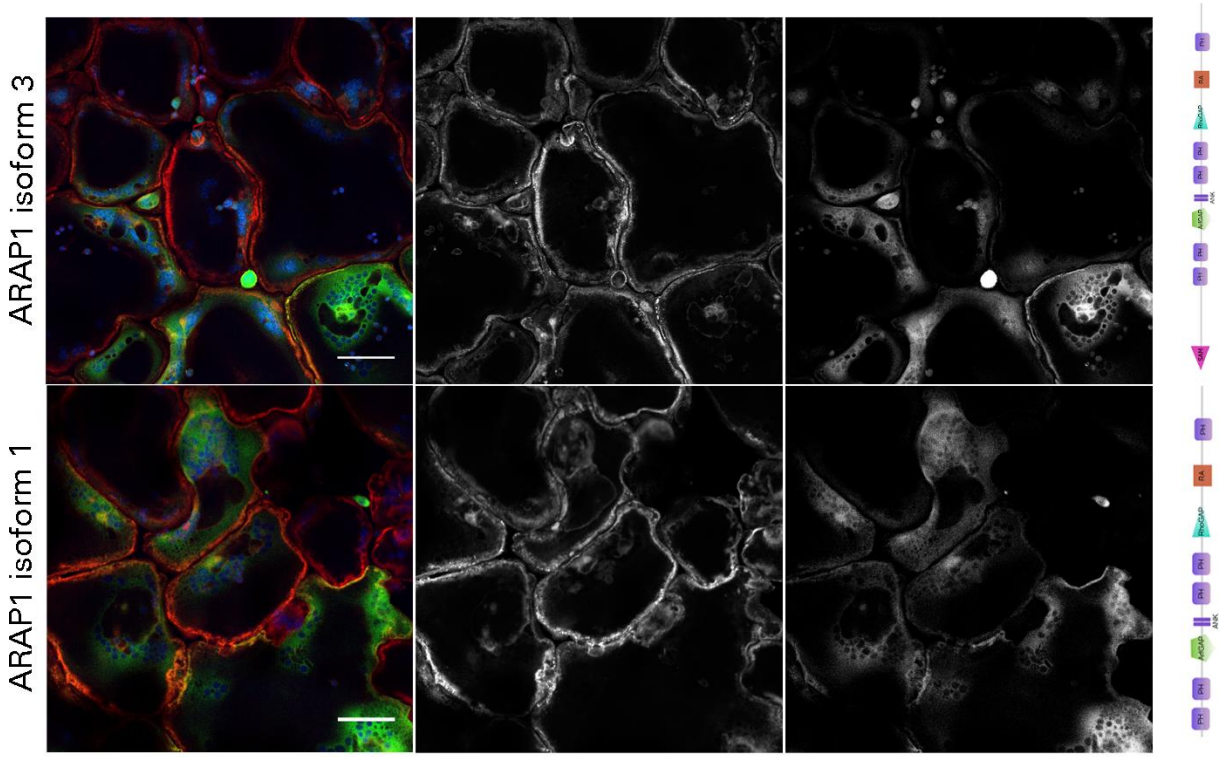

Supplemental figure 3

Figure S3. Overexpression of different ARAP1 isoforms. Related to Figure 2.

Osteoclasts overexpressing GFP-ARAP1-isoform 1 and 3 were grown on glass, fixed and stained with actin (red) and DAPI (blue). Images were analyzed using the Fiji software.

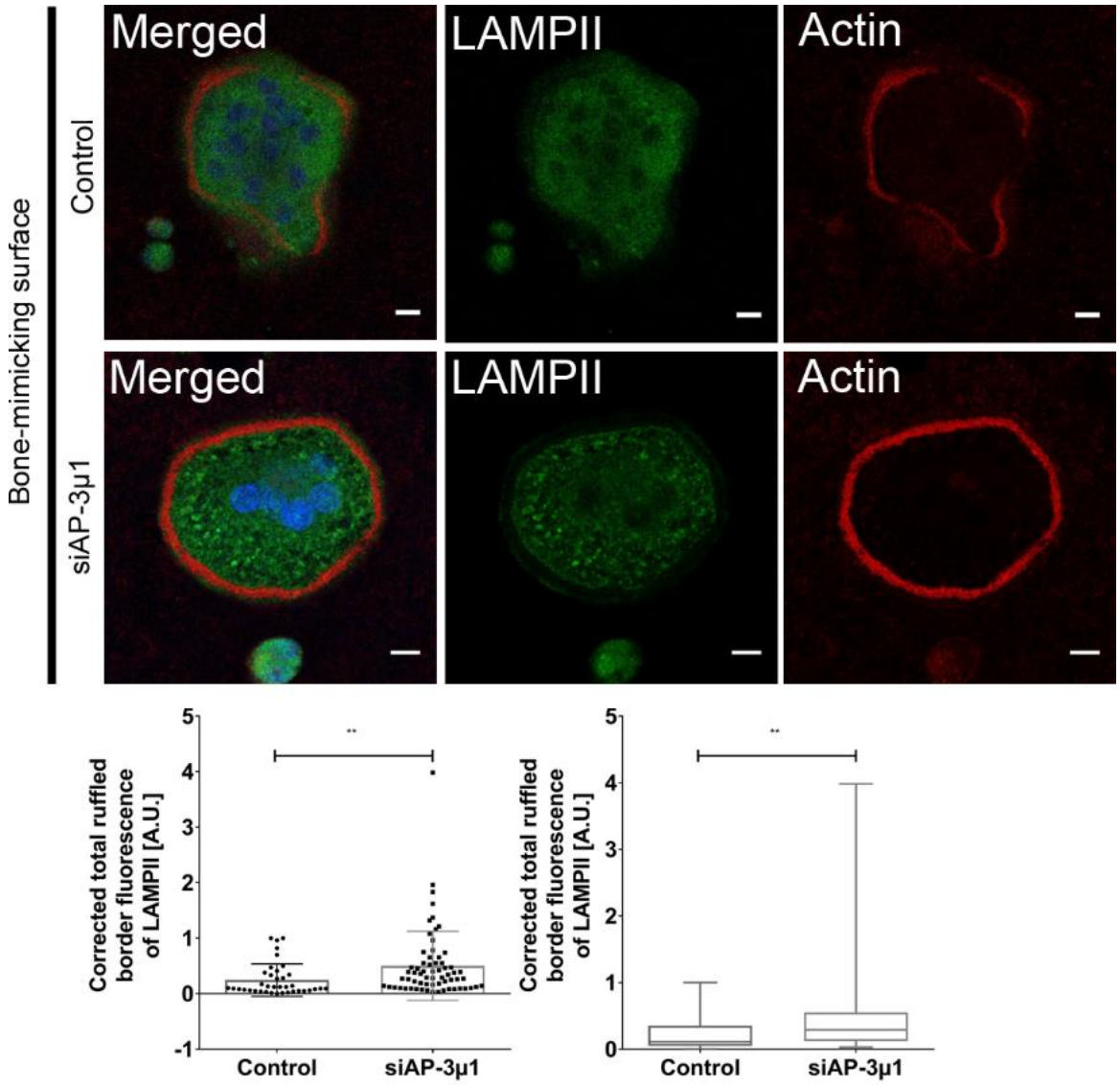

Supplemental figure 4

Figure S4. AP-3 depleted osteoclast and LAMPII at the ruffled border. Related to Figure 5.

Osteoclasts were depleted in ARAP1 as previous described. Cells on ACC were fixed and stained for phalloidin (red) and LAMPII (green). As in Fig.5, the relative LAMPII fluorescence intensity at the ruffled border in AP-3µ1 KD was measured and plotted as a Box and Scatter--plot (n=3, mean ± SD; student's t-test, **** p<0.0001). The large error bars can be explained by variations in the knockdown efficiency in individual osteoclasts.

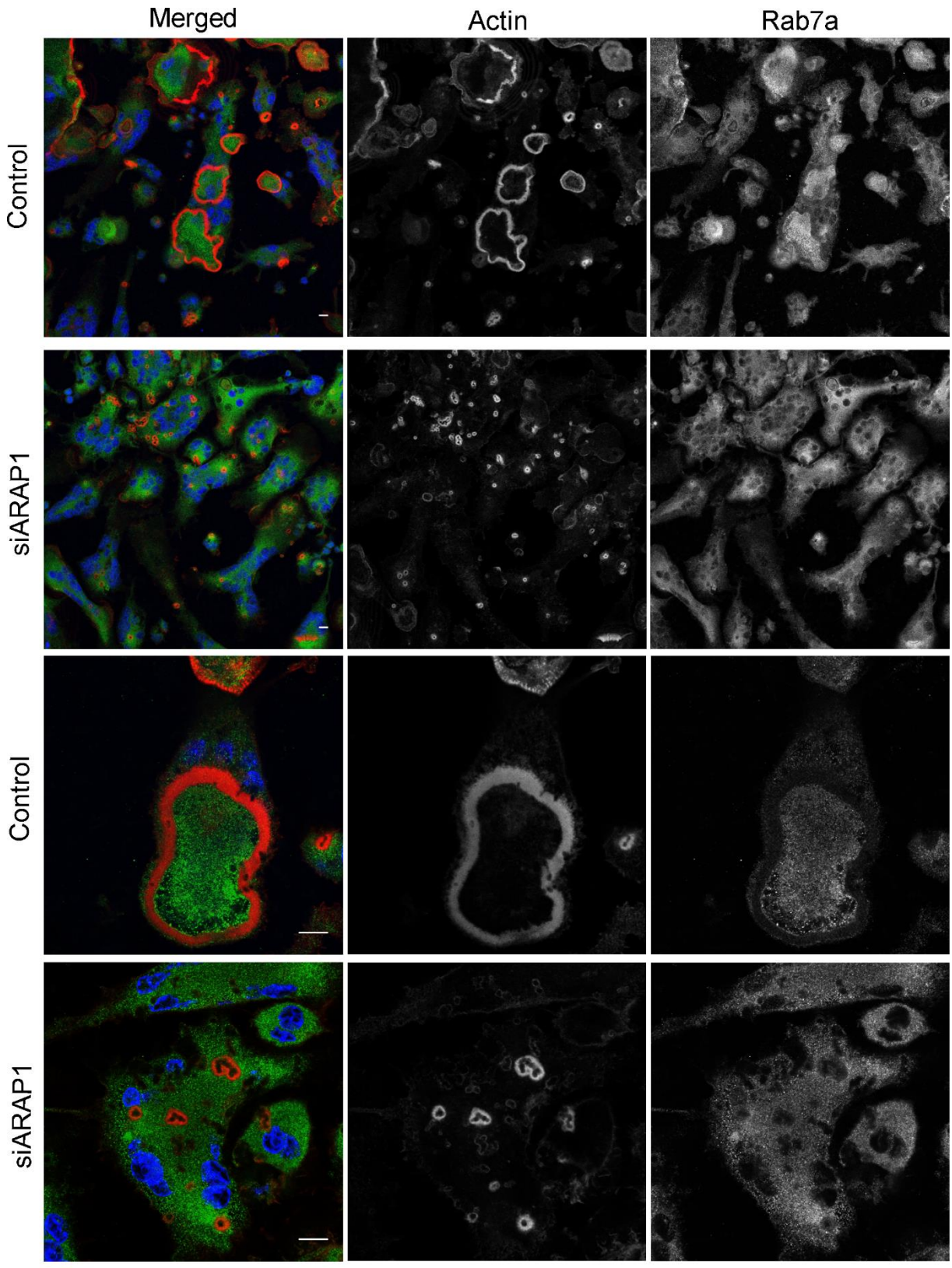

Supplemental figure 5

Figure S5. Effect of ARAP1 KD on Rab7 distribution in osteoclast. Related to Figure 5.

Osteoclasts treated with siARAP1 or mock siRNA were grown on glass or ACC, fixed and stained with Phalloidin (red), Rab7a (green), DAPI (blue). (scale bar: 10μm)

Transparent Methods

Reagents

Primary antibodies: goat-anti-ARAP-1 (immunofluorescence (IF) 1:50) (Abcam); rabbit-anti-AP3s1 (IF 1:250) (Aviva); mouse-anti-AP3d1 (IF 1:250, Western blot (WB): 1:1000 (Acris Antibodies); anti-mouse Lamp-1 (CD107b) (IF 1:250, WB 1:1000); rabbit-anti-Vps35 (IF 1:250) (Millipore); rabbit-anti-EEA1 antibodies were kindly provided by Prof. Marino Zerial, Max Planck Institute of Molecular Cell Biology and Genetics, Dresden, Germany; anti-GM130 (IF 1:250) (BD Bioscience); anti-Rab7A (IF 1:250) (Sigma Aldrich); rabbit- anti-GAPDH (WB 1:5000) (Bioss Antibodies). Secondary antibodies: Horse-radish peroxidase (HRP)-conjugated goat anti-mouse IgG, goat anti-rabbit IgG, mouse anti-goat IgG, donkey anti-rat IgG (WB 1:5000-1:10000) (Jackson Immuno Research Laboratories), Alexa Fluor 488, 546, 633-conjugated against the corresponding primary antibodies (IF 1:250) (Molecular Probes, Invitrogen), Phalloidin-Alexa-546 or Phalloidin-Alexa-633 (IF 1:300) (Life Technologies), DAPI (IF 10 µg/mL) (Life Technologies).

Cell culture

Raw264.7 cells (ATCC #TIB-71) were cultivated at 37°C under a humidified 5% CO2 atmosphere in Dulbecco's modified Eagle medium (DMEM)-GlutaMAX-I (Life Technologies) supplemented with 10% (v/v) Fetale Bovine Serum (Biochrom), 2 mM L- glutamine, 0.1 mg/ml streptomycin and 100 U/ml penicillin-G (Life Technologies). Upon treatment with RANKL (self made) for in vitro osteoclastogenesis, cells were grown in Alpha-minimum essential media (α-MEM) (Biochrom) supplemented with 10% (v/v) Fetale Bovine Serum (Biochrom), 2 mM L-glutamine, 0.1 mg/ml streptomycin and 100 U/ml penicillin-G (Life Technologies). For microscope analysis and RNA intereference, differentiated cells were washed 2 times with PBS and incubated for 5-10 min with PBS to remove undifferentiated mononucleated cells. Then osteoclasts were detached with a cell lifter (Corning Incorporated Costar), centrifuged at 250xg for 5 min, resuspended in α-MEM 2% RANKL, and then transferred either to glass cover slips (∅ 11mm) or Apatite-collagen complexes (ACC), Ibidi µm, 35mm, glass bottom dish, ACC coated chambers, Osteoassay dishes™ or subjected to electoporation. Soluble recombinant RANKL was produced in Pichia yeast as described previously (Czupalla et al., 2005).

Apatite-collagen complexes (ACC) slide preparation

ACCs were produced as described by Shitbutani et.al and others (Saltel et al., 2004, Shibutani et al., 2000, Doi et al., 1996). Briefly, glass slides (∅ 11mm) were coated with rat-tail type I collagen (Corning) over night and washed with 200 mM Tris-buffered saline (TBS). Then, slides were incubated for 6 days at 37°C in 200 mM TBS containing 0.013 mg/mL alkaline phosphatase (Applichem), 0.13 mg/mL egg-yolk phosvitin (Sigma) and 1 mg/mL dimethyl suberimidate hydrochloride (Sigma). The crosslinked, collagen-coated glass slides were then washed 3 times with TBS to remove unreacted chemicals and by-products. These glass slides were incubated for 4 h hat 37°C in 200 mM TBS containing alkaline phosphatase (0.13 mg/mL) and phosvitin (0.13 mg/mL). Then they were incubated for 20 h at 37°C with 6 mM calcium β-glycerophosphate (Sigma) solution buffered at pH 8.5 with 200 mM TBS. The 4- and 20-h incubations were repeated 1–10 times, depending on the amount of precipitated calcium phosphate. After washing with TBS, the surface of uncoated side was cleaned with 0.1 M HCl solution to remove the precipitate. The glass slides was then dried and sterilized under UV light.

RNA interference

Predesigned Stealth siRNA (Life Technologies) or a Negative Control Medium GC stealth siRNA (Life Technologies) were electroporated into differentiated osteoclast in Electroporation Iso-osmolar Buffer (Eppendorf) with a single square wave pulse of 2,500 V/cm field strength and 300 µs pulse length using an ECM830 ElectroSquarePorator (BTX). Electroporated

osteoclasts were resuspended in α-MEM supplemented with RANKL and allowed to recover for 46 h. Osteoclasts were processed for subsequent analysis.
Pre-designed Stealth stealth, siRNA sense sequences (Thermo Fischer Scientific) (5' to 3'); ARAP1: AGGUGGAGACUGAACAGCAUGUUAA; CAUCUGGGCAUUGGUAUCACCUUUA
AP-3 m1: UCCCAAGUCUUAAAGGACUAGUAAA; UGGUGAGAAGUAUAAGCCAUUUAAA

Adenovirus production and gene transduction

The cDNA of murine ARAP-1 transcript variant 3 was obtained from GeneCopeia™. Recombinant adenoviruses were generated using the AdEasy™ system (Qbiogene) developed by He et al. (He et al., 1998). The pShuttle-CMV vector was recombined with the pAdeasy-1 plasmid in BJ5183 cells (Stratagene). Vectors linearized with PacI were transfected into the packaging cell line HEK293A (Qbiogene) and amplified until the virus was purified with an Optiprep™ gradient (Sigma Aldrich). Osteoclasts were transduced 4 days after differentiation with 200 pfu/cell adenovirus and grown for additional 48 h either on ACCs or glass coverslips. Cells were then processed for subsequent analysis.

Immunofluorescence and Confocal Laser Scanning Microscopy

Osteoclasts grown on glass or ACCs were fixed with 4% (w/v) paraformaldehyde in PBS for 15 min at 37°C and subsequently permeabilized with 0.1% (w/v) Triton X-100 in PBS for 10 min. Samples were blocked with 3% (w/v) BSA in PBS for 1 h at RT, followed by incubation with primary antibodies diluted in 3% (w/v) BSA in PBS for 1 h at room temperature. After washing, cells were incubated with an appropriate secondary antibody. Glass coverslips and ACCs were washed and mounted on glass slides with Mowiol (Sigma) containing. Slides were imaged with a LSM-700 (Zeiss) equipped with the following objectives: Zeiss Plan-Apochromat 10x 0.45, Zeiss Plan-Apochromat 20x 0.8, Zeiss C-Apochromat 40x 1.2 W, Zeiss Plan Neofluar 40x 1.3 oil, Zeiss Plan-Apochromat 100x 1.4 Oil, Zeiss Plan-Apochromat 63x 1.4 Oil.For resorption pit analysis dishes and slides were imaged using a Axio Observer.Z1 (Zeiss) equipped with a Zeiss EC Plan Neofluar 2.5x 0.075 objective. Image analysis was done using Fiji (Image J) and the ZEN 2010 software. For measuring the corrected total cell fluorescence (CTCF) complete osteoclasts or their respective ruffled borders (RB) were imaged and the cell of interest/ RB of interest was selected using the Fiji drawing tool. The region of interest and background was measured to calculate the area and the integrated intensity. The CTCF was calculated using the following formula: CTCF = Integrated Density - (Area of selected cell X Mean fluorescence of background readings). During the image aquisition and during post-processing all parameters were kept constant.

Resorption pit analysis

Cells that underwent knockdown were seeded onto a 24-well osteoassay dish (Corning) (80.000 cells/well) and grown for 46 hours for recovering and resorption. Osteoclasts were detached with ~6% NaOCl and ~5.2% NaCl for 5 mins, the wells were rinsed with water and dried. A tile scan of the wells was made with an inverted Axio Observer.Z1 (Zeiss). Tiles were stitched with the ZEN 2010 software and analyzed for the percentage of the resorbed area using the Fiji software.

Quantitative PCR

Total RNA was isolated from osteoclasts by using the Quick-RNA™ MicroPrep (Zymo Research), and reverse transcription was performed using the M-MLV Reverse Transcription system (Promega). Quantitative RT-PCR (QPCR) was performed with a Stratagene Mx3000 system and the Brilliant II SYBR green QPCR kit according to the manufacturer's instructions (AgilentTechnologies).

Primers:
GAPDH FW:AGGTCGGTGTGAACGGATTTG; RV:TGTAGACCATGTAGTTGAGGTCA

AP-3m1 FW: CCGTTCCGCTCGTTGTGTC; RV: GGATCATTTTCCCGACACCTG

Immunoprecipitation and Western blotting

For immunoprecipitation, osteoclasts were lysed using ice-cold lysis buffer (50 mM Tris-HCl pH 7.4, 150 mM NaCl, 1.0% Triton X-100, 0.1% sodium deoxycholate, 1 mM EDTA plus protease and phosphatase inhibitors). For immunoprecipitations of proteins, lysates were precleared on Protein G-magnetic beads (Carl Roth) for 1 h at 4°C. Protein G-beads were incubated with antibodies for ON at 4°C. Then, precleared supernatants were added for 1 h at 4°C. Precipitates were washed two times with 0.05% Tween-20; proteins were eluted, and resolved by SDS-PAGE.

For Western blotting equal amounts of osteoclast extracts (10-20µg) were subjected onto a SDS-PAGE and resolved, then wet-blotted onto nitrocellulose membranes, and subsequently incubated with primary antibodies. After incubation with secondary antibody, bands were detected with enhanced chemiluminescence Western blotting detection reagents (Amersham). Densitometric quantification of Western blots was performed by using ImageJ software (National Institutes of Health).

Mass spectrometry-based protein identification and quantification

Entire gel lane was cut into 11 slabs each of which was in-gel digested with trypsin and analysed individually. Peptides recovered from in-gel digests were dissolved in 15 µl of 5% aqueous formic acid spiked with 10 fmol of Glu-1 Fibrinopeptide B (reference standard for alignment and normalization of chromatograms). A 5 µl aliquot of the peptide digest was analyzed by LC-MS/MS on an Ultimate3000 nanoLC systems (Dionex, Amsterdam, The Netherlands) equipped with a 75 µm i.d. x 20 mm trap column and 75 µm x 15 cm analytical column (Acclaim PepMap100 C18 3µm/100A, both from Dionex) interfaced on-line to a LTQ Orbitrap Velos hybrid mass spectrometer (Thermo Fisher Scientific, Bremen, Germany). A 180 min elution program was applied utilizing 0.5% aqueous formic acid as solvent A and neat acetonitrile as solvent B. The data-dependent acquisition (DDA) cycle consisted of FT MS survey spectrum followed by 6 MS/MS spectra with a fragmentation threshold of 5 000 ion counts and dynamic exclusion time of 25s, singly charged and charge-unassigned precursor ions were excluded. FT survey scans were acquired within m/z range of 300 to 1700. Lock mass was set to the singly charged ion of dodecamethylcyclohexasiloxane ion ($(Si(CH_3)_2O))_6$; m/z = 445.120025).

Spectra were converted to mgf format using extract_msn converter (ver.5, Thermo Fisher Scientific, Bremen, Germany) and mgf's obtained for individual gel slabs were merged. Proteins were identified by Mascot v.2.2.04 software (Matrix Sciences, UK) searching against mouse sequences in the NCBI protein sequences database (compiled in April 2015, 173761 entries) under the following settings: 5 ppm and 0.5 Da mass accuracy on precursor and fragment ions correspondingly; enzyme specificity: trypsin; number of allowed miscleavage sites: two; variable modifications: methionine oxidized, cysteine propionamide, cysteine carbamidomethyl, protein N-terminal acetyl. The result of the database search was evaluated by Scaffold software (Proteome Software, Portland, US, v.4.3.4) under the following settings: minimal number of matching peptide was set as 2; peptide and protein probabilities thresholds were 95% and 95% correspondingly. Calculated False Discovery Rates (Scaffold standard feature) were below 0,0% for peptides and 0,83% for spectra.

Integration of chromatographic peaks of peptides was performed by Progenesis software (NonLinear Dynamics, Newcastle, UK). Relative abundance of proteins was calculated as sum of integrals of all peptides matched to the protein sequence normalized to total protein abundance using in-house written scripts.

Animals

Heterozygous *mocha* mice were originally obtained from M. Robinson (Cambridge Institute for Medical Research, Cambridge, U.K.) and then bred in-house. The experiments were carried out in accordance with the European Community Council Directive of November 24, 1986 (86/609/EEC). All efforts were made to minimize the number of animals used and their suffering.

Micro Computed Tomography

Mouse tibias were scanned on a Skyscan 1072 (Bruker microCT, Belgium) using a voltage of 50kV/190uA and 0.5mm Aluminium filter and magnification of x58 (pixel size 5.05um). These were then reconstructed using NRECON software (Bruker microCT, Belgium) using the same threshold settings for all bones. 200 slices of the reconstructed data was selected and a ROI drawn to select the trabecular bone, analysis was then carried out using CTAn software (Bruker microCT, Belgium).

Supplemental references

CZUPALLA, C., MANSUKOSKI, H., PURSCHE, T., KRAUSE, E. & HOFLACK, B. 2005. Comparative study of protein and mRNA expression during osteoclastogenesis. *Proteomics,* 5**,** 3868-75.

DOI, Y., HORIGUCHI, T., MORIWAKI, Y., KITAGO, H., KAJIMOTO, T. & IWAYAMA, Y. 1996. Formation of apatite-collagen complexes. *J Biomed Mater Res,* 31**,** 43-9.

HE, T. C., ZHOU, S., DA COSTA, L. T., YU, J., KINZLER, K. W. & VOGELSTEIN, B. 1998. A simplified system for generating recombinant adenoviruses. *Proc Natl Acad Sci U S A,* 95**,** 2509-14.

SALTEL, F., DESTAING, O., BARD, F., EICHERT, D. & JURDIC, P. 2004. Apatite-mediated actin dynamics in resorbing osteoclasts. *Mol Biol Cell,* 15**,** 5231-41.

SHIBUTANI, T., IWANAGA, H., IMAI, K., KITAGO, M., DOI, Y. & IWAYAMA, Y. 2000. Use of glass slides coated with apatite-collagen complexes for measurement of osteoclastic resorption activity. *J Biomed Mater Res,* 50**,** 153-9.